Influence of local anisotropic magnetoresistance on the total magnetoresistance of mesoscopic NiFe rings

Dieter Buntinx, Alexander Volodin, and Chris Van Haesendonck
Laboratorium voor Vaste-Stoffysica en Magnetisme, Katholieke Universiteit Leuven, Celestijnenlaan 200 D, B-3001 Leuven, Belgium
(Received 10 October 2003; revised manuscript received 17 March 2004; published 7 December 2004)

The magnetoresistance of mesoscopic NiFe rings is studied by low temperature magnetotransport measurements and numerical simulations. In order not to disturb the magnetic states in the electrical transport measurements, nonmagnetic gold wires are attached to individual rings. The simulations compute the change in resistance that is caused by the anisotropic magnetoresistance (AMR) effect and are based on a combination of magnetostatics for the magnetic domain configuration and electrostatics for the current distribution. Measurements as well as simulations reveal the presence of two stable "onion" states at remanence and a stable "vortex" state near the switching fields. Moreover, a quantitative comparison between experiment and simulation is possible without the use of any free fitting parameters. Apart from the AMR effect, no additional domain wall resistance has to be introduced for the onion state. In the switching region, experiment and simulation reveal the presence of a "stressed vortex" configuration which plays a key role in the quantitative description of the magnetoresistance. The switching behavior of the NiFe rings can be modified by introducing a wedge shaped notch at the expected position of one of the domain walls in the onion state of the rings.

DOI: 10.1103/PhysRevB.70.224405 PACS number(s): 75.60.−d, 72.15.Gd, 75.30.Gw, 75.40.Mg

I. INTRODUCTION

During the last few years, mesoscopic ferromagnetic ring structures were studied intensively because of their interesting ferromagnetic properties.[1–5] The shape anisotropy in the narrow rings induces two stable ferromagnetic states. An onion state is stable at remanence and can be accessed by saturation of the magnetization. This state is characterized by two opposite head-to-head domain walls. A flux-closure state or vortex state occurs in the vicinity of the switching fields. In this case the domain walls disappear and the magnetization runs continuously throughout the ring. Because of their particular magnetic properties, the rings are well suited to study fundamental magnetic properties, including magnetization reversal, domain wall trapping and magnetoresistance.

Arrays of rings were intensively studied by magnetization measurements as well as by micromagnetic simulations. This way, the influence of the geometry and the thickness on the switching fields was identified. By introducing notches along the ring circumference, one is able to tune the switching of the rings from the onion state to the vortex state. The different magnetic states of the rings were visualized by magnetic force microscopy and Hall probe microscopy.[5,6] Recently, isolated rings were studied by magnetotransport measurements and Hall magnetometry.[2–5] In this article, we present our study of isolated NiFe rings using magnetoresistance measurements and numerical simulations. We show that the measured change in resistance can be compared quantitatively with simulations that are based on the anisotropic magnetoresistance (AMR) effect.[7] Switching from the onion state to the vortex state, the resistance change is mainly caused by the annihilation of the two head-to-head domain walls of the onion state. This way a detailed quantitative analysis of the resistance caused by the domain walls is possible. An essential ingredient in the understanding of the magnetoresistance is the introduction of a stressed vortex configuration. Finally, we demonstrate how the introduction of a notch influences the switching behavior. In order not to disturb the magnetic states of the rings, nonmagnetic gold wires are attached to all the individual rings for the electrical measurements.

II. FABRICATION

The rings and the nonmagnetic contacts are fabricated by combining electron beam lithography and lift-off techniques. In a first step, a ring with inner radius of 2 μm and outer radius of 2.5 μm is written into a double resist layer which is spin coated on an oxidized silicon substrate. After development a 35 nm thick permalloy (80%Ni, 20%Fe) layer is deposited in a molecular beam epitaxy (MBE) system with a base pressure of 10^{-10} mbar. Next, the substrate is immersed in a hot bath of acetone for the lift-off. In a second step, the same procedure together with a very precise alignment is used to attach to the NiFe rings nonmagnetic gold contacts with a width of 0.5 μm and a thickness of 20 nm. To improve the adhesion of the Au to the oxidized silicon substrate, a 2 nm thick Ti layer is first deposited. Figure 1(a) shows a scanning electron microscopy image of a regular NiFe ring with the attached gold contacts. A second ring containing a single notch at the expected position of one of the domain walls in the onion state is shown in Fig. 1(b). The magnified image of the notch shows that it is wedge shaped and extends as far as half the width of the ring.

III. EXPERIMENT AND SIMULATION

A. Regular ring

The magnetoresistance of the rings is measured using a four-terminal ac technique with lock-in detection. The ring is fed with a current having a frequency of 27 Hz and a root-mean-square (rms) amplitude of 3.5 μA. The temperature is

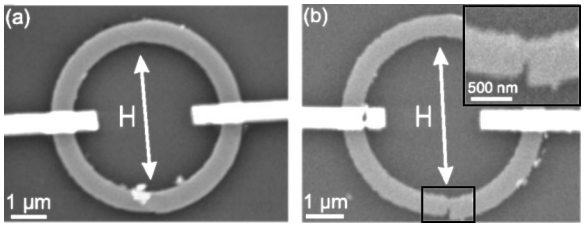

FIG. 1. Scanning electron micrographs of a regular ring (a) and a notched ring (b). The white arrows indicate the direction of the external magnetic field with respect to the rings while the inset in (b) shows a magnified image of the notch.

fixed at 10 K (±10 mK), while the magnetic field is applied in the vertical direction within the plane of the ring (see Fig. 1). The magnetoresistance of the regular ring is shown in Fig. 2(a), where the magnetic field is swept from 0.5 to −0.5 T. A total resistance change of approximately 2.15 Ω is observed, which is about 1.7% of the resistance of the ring in saturation ($R=128\ \Omega$). In Fig. 2(b) a more detailed view of the magnetoresistance near zero field is shown for the regular ring (upper continuous curve) as well as for the notched ring (lower continuous curve). After applying a saturating field of 0.5 T, a field sweep is performed from 45 to −45 mT with field steps of 0.05 mT. The switching region can be clearly recognized in the vicinity of −25 mT. At positive fields the ring remains in the onion state with two opposite head-to-head domain walls. In the switching region, the first jump corresponds to the transition from the onion state into the vortex state. After a steep decrease in the resistance, a second smaller jump indicates the transition from the vortex state into the onion state with opposite magnetization. The height of this second jump is enhanced for the notched ring when compared to the regular ring. For a further discussion of the notched ring, we refer to the next paragraph.

The resistance changes in Fig. 2 can be explained in terms of the anisotropic magnetoresistance (AMR) effect.[7] The resistivity depends on the angle α between current and magnetization: $\rho=\rho_\perp+(\rho_\parallel-\rho_\perp)\cos^2\alpha$, where $\rho_\perp$ and $\rho_\parallel$ are the resistivity for $\alpha=90°$ and $\alpha=0°$, respectively. Therefore, it is necessary to know the current distribution as well as the local magnetization. The latter is calculated using micromagnetic simulations.[8] The simulations are based on the integration of the Landau-Lifshitz-Gilbert equation. Because our rings are made out of polycrystalline NiFe, the crystalline anisotropy term can be neglected. The material parameters used for the simulations are a saturation magnetization $M_s=8.6\times10^5$ A/m and an exchange (stiffness) constant $A=1.3\times10^{-11}$ J/m. The ring is divided into a two-dimensional square mesh containing three-dimensional spins. The lateral cell size is 12.5×12.5 nm^2, while the damping coefficient α is equal to 0.05. Figure 3 shows the calculated local magnetization for a regular ring at different magnetic fields. For a field of 0.55 T [Fig. 3(a)], the magnetization reaches saturation. All the magnetic moments point in the direction imposed by the external magnetic field. When decreasing the field towards zero, the moments start to align with the border of the ring because of the shape anisotropy, and the ring will be in one of the onion states with two distinct head-two-head

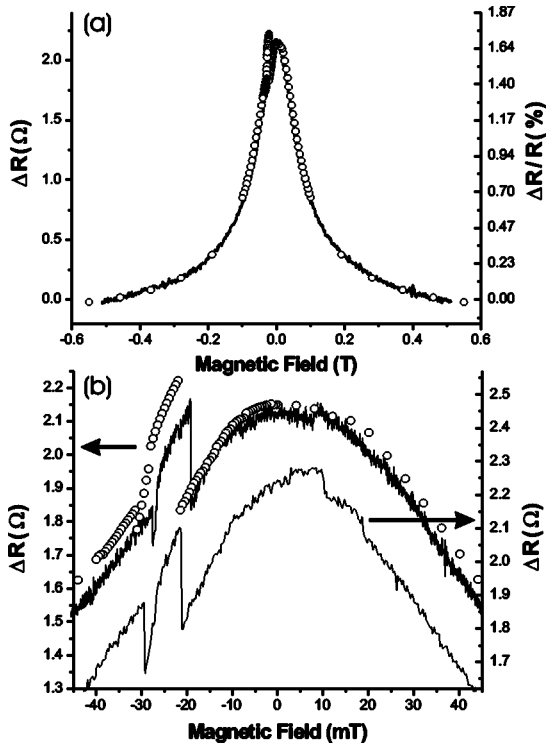

FIG. 2. Magnetoresistance of a regular NiFe ring for larger magnetic fields [continuous curve in (a)], and close to zero field [upper continuous curve in (b)]. The open circles correspond to the calculated magnetoresistance based on the AMR effect. The lower continuous curve in (b) gives the experimental magnetoresistance for the notched ring. Note the different scale for the two rings (see arrows).

domain walls. When further decreasing the field, the onion state remains stable. In Fig. 3(b) the onion state is shown at remanence. A careful analysis of the simulated magnetization reveals a vortex-like configuration of the magnetic moments in the domain walls, consistent with the behavior expected[9] from the width and the thickness of our rings. We note that the shape induced vortex-like domain walls have a width (≈500 nm) which is considerably larger than the usual domains walls appearing in larger NiFe films. At a field of −22 mT, the ring switches into the vortex state, where no domain walls are present. In the simulations the transition to the vortex state can occur either by the reversal of the left or the right half of the ring. Figure 3(c) shows the stable vortex state at a field of −24 mT. At larger negative values of the field, the magnetic moments in the right half of the ring that have not yet been reversed, feel an increasing and opposite external field. In Fig. 3(d) the vortex state is shown for −31 mT. Because of the external field, the moments on the right side of the ring form a zigzag pattern in order to lower their energy. We refer to this feature as the stressed vortex configuration, which to our knowledge has not been described before. The stability of this new configuration is confirmed by micromagnetic simulations for a cell size down to 5 nm, which is comparable to the exchange length of NiFe. Finally, at a field of −31.5 mT the ring switches into the second onion state [Fig. 3(e)]. When further increasing the field, saturation is again reached. In Fig. 4(e) the corresponding simulated hysteresis loop can be found.

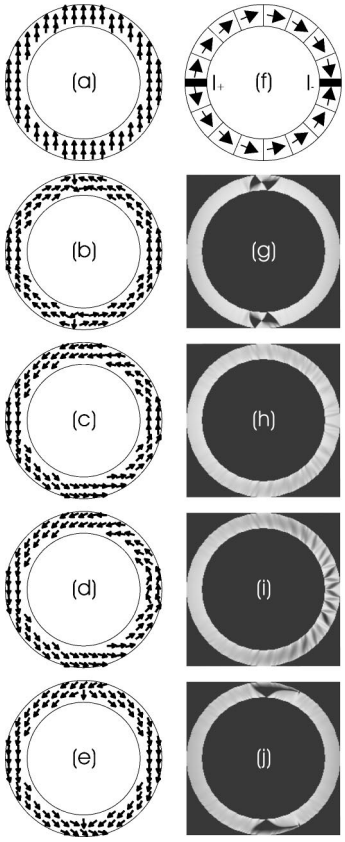

FIG. 3. Simulated configuration of the magnetization of the regular ring at different values of the applied magnetic field. (a) 0.55 T (saturated state), (b) 0 T (onion state), (c) −24 mT (vortex state), (d) −31 mT (stressed vortex configuration) and (e) −31.5 mT (second onion state). In (f) the equipotential lines and the current distribution are shown. In (g)–(j) the calculated local resistivity is plotted corresponding to configurations of the magnetization shown in (b)–(e), respectively.

To calculate the AMR related change in resistance corresponding to the simulated variations in the magnetization, it is necessary to know the current distribution inside the ring. From electrostatics we know that the current flows in a direction perpendicular to the equipotential lines. Figure 3(f) shows the equipotential lines and the current direction for a regular ring when a voltage is applied between the two gold contacts. We assume the finite width of the gold contacts does not disturb the current distribution. A second approximation is that local resistivity changes due to the AMR effect are neglected when calculating the current distribution. Knowing the local magnetization and the current direction, i.e., the angle α between the current and the magnetization, the local magnetoresistivity in the ring can be calculated. The only parameters needed are $\rho_\perp$ and $\rho_\parallel$, which are determined experimentally by measuring a reference sample which is simultaneously deposited with the ring. We find $\rho_\perp = 1.56 \times 10^{-7}\ \Omega$m and $\rho_\parallel = 1.63 \times 10^{-7}\ \Omega$m, corresponding to an AMR ratio $\Delta\rho/\rho_\perp = (\rho_\parallel - \rho_\perp)/\rho_\perp = 4.3\%$. In Figs. 3(g)–3(j) we show plots of the local AMR resistivity corresponding to the distribution of the magnetization shown in Figs. 3(b)–3(e), respectively. Lighter regions correspond to a higher resistivity, while darker regions correspond to a lower resistivity. The head-to-head domain walls in the two different onion states [Figs. 3(g) and 3(j)] clearly correspond to regions of low resistivity. Inside the domain walls the magnetic moments and the current point into different directions, explaining the reduced resistivity. In the other parts of the ring the resistivity is higher because the magnetic moments tend to align parallel to the current. In the vortex state [Fig. 3(h)] the domain walls disappear and the resistivity becomes more homogeneous throughout the ring. Figure 3(i) nicely illustrates that the zigzag pattern of the stressed vortex configuration [Fig. 3(d)] results in a local reduction of the resistivity.

By integrating the local resistivity over the entire ring, the total resistance of the ring can be calculated as a function of the external magnetic field. This calculation is performed for 140 different magnetic fields. The calculated magnetoresistance values are added as open circles to the magnetoresistance plots in Figs. 2(a) and 2(b). For convenience, the resistance is set to zero at a field of 0.5 T for both the experiment and the simulation. On a larger field scale [Fig. 2(a)], there is a nearly perfect quantitative agreement between experiment and simulation. The total resistance change between saturation and remanence is 2.15 Ω in the experiment and 2.26 Ω in the simulation. Figure 2(b) shows a more detailed plot of the magnetoresistance around zero field. Starting from 45 mT, experiment and simulation nearly coincide until reaching the switching region. According to the simulation, the switching to the vortex state occurs at −22 mT and the height of the corresponding resistance jump is 0.39 Ω. The experimental switching field of the regular ring is −19 mT with a resistance jump having an average height of $0.31\ \Omega \pm 0.02\ \Omega$ (averaging over 14 measurements). Since the removal of the onion state domain walls results in an increase of the resistance, one can conclude that the appearance of the domain walls results in a decrease of the resistance. Moreover, our simulations indicate that the AMR effect provides a quantitative description of the resistance decrease and no additional intrinsic domain wall resistance has to be introduced. This is in disagreement with previous experiments[10] that report on a negative intrinsic domain wall resistance for shape induced domain walls. The absence of intrisic domain wall resistance can be understood in terms of the larger width of the domains walls which allows the conduction electrons to fully track the changing magnetization direction inside the domain walls.[11] When further increasing the field towards more negative values, the experimental and simulated magnetoresistance decreases with an almost identical slope. From the local resistivity plots, we know that this decrease is caused by the formation of the stressed vortex configuration with a zigzag pattern of the magnetization. This decrease continues until the ring switches into the second onion state. The simulated transition to the onion state takes place at −31.5 mT with a second smaller jump in the resistance. Experimentally, the onion state with reversed magnetization nucleates for the regular ring at −27.6 mT with an almost identical jump. The experimental and simulated width of the vortex state is 8.6 and 9.5 mT, respectively.

B. Notched ring

The magnetoresistance of the ring with the notch [Fig. 2(b)] behaves very similar until reaching the second switching field. The height of the jump at the first switching field matches very well for both rings. Also, the field range for the existence of the vortex state is comparable. The main difference between both rings is the increased height of the second jump into the reversed onion state for the notched ring. Micromagnetic simulations of the notched ring and the regular ring shown in Fig. 4 reveal that this can be explained by a combination of two effects. First, comparing Figs. 4(a) and 4(b), the introduction of the notch results in a more pronounced zigzag pattern of the magnetization, resulting in a lower resistance of the stressed vortex configuration just before the jump. Second, there is a difference in the onion states after switching has occurred. Because the notch is introduced at the expected position of one of the two head-to-head domain walls for the regular ring, this domain wall emerges next to the notch. This results in an asymmetric onion state with a slightly increased resistance [Figs. 4(c) and 4(d)]. Finally, the calculated hysteresis loop of the notched ring has been added to Fig. 4(e) and can be compared to the corresponding hysteresis loop of the regular ring.

IV. CONCLUSION

We measured the low temperature magnetoresistance of mesoscopic NiFe rings. The results are compared to numerical simulations which take into account the contribution of the AMR effect to the magnetoresistance. In the calculation no adjustable fitting parameters are used. The nice agreement between simulation and experiment indicates the AMR is the dominating source of magnetoresistance. From the comparison between measurement and simulation we can conclude that (i) the stressed vortex configuration is essential to obtain a quantitative description of the resistance behavior and (ii) no intrinsic domain wall resistance has to be introduced to explain the resistance of the onion state. Introducing a notch along the ring circumference results in a modified switching behavior that can be linked to a more pronounced stressed vortex configuration and a shift in the position of one of the domain walls. In the future, similar techniques will be used to understand the contribution of the AMR effect to the magnetoresistance of other, more complicated mesoscopic ferromagnetic structures. In order to obtain an improved description of the current distribution, more advanced finite element calculations will be used, incorporating the influence of local resistivity changes due to the AMR effect on the current distribution.

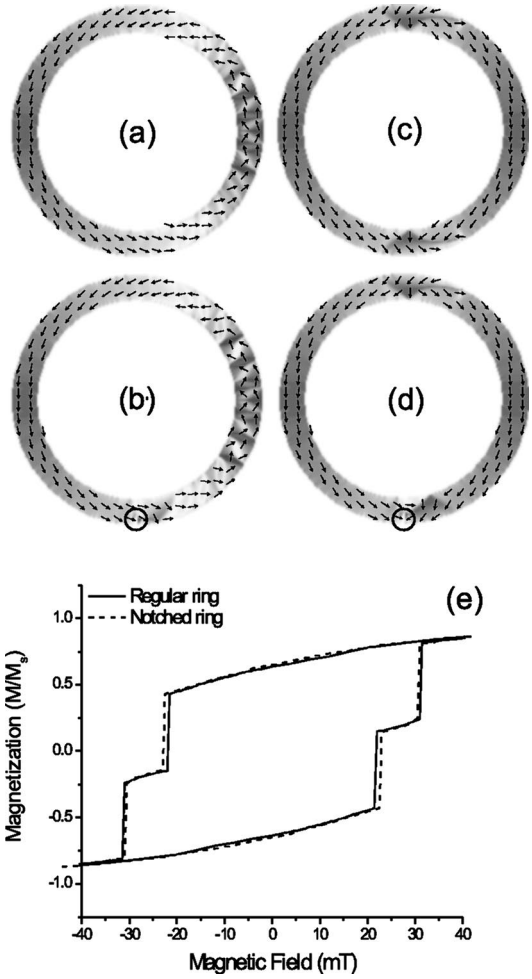

FIG. 4. Micromagnetic simulations of the regular ring [(a) and (c)] and the notched ring [(b) and (d)] just before and just after the switch from the stressed vortex configuration into the 'onion' state. The encircled areas indicate the location of the notch. The white and black contrast reflects the magnitude of the horizontal and vertical component of the magnetization, respectively. In (e) the hysteresis loop obtained from the micromagnetic simulations is shown for the regular ring as well as for the notched ring.

ACKNOWLEDGMENTS

This work has been supported by the Fund for Scientific Research - Flanders (FWO) as well as by the Flemish Concerted Action (GOA) and the Belgian Interuniversity Attraction Poles (IAP) research programs.

[1] J. Rothman, M. Kläui, L. Lopez-Diaz, C. A. F. Vaz, A. Bleloch, J. A. C. Bland, Z. Cui, and R. Speaks, Phys. Rev. Lett. **86**, 1098 (2001).

[2] M. Kläui, C. A. F. Vaz, J. A. C. Bland, W. Wernsdorfer, G. Faini, and E. Cambril, Appl. Phys. Lett. **81**, 108 (2002).

[3] M. F. Lai, Z. H. Wei, C. R. Chang, J. C. Wu, J. H. Kuo, and J. Y. Lai, Phys. Rev. B **67**, 104419 (2003).

[4] M. Kläui, C. A. F. Vaz, J. Rothman, J. A. C. Bland, W. Wernsdorfer, G. Faini, and E. Cambril, Phys. Rev. Lett. **90**, 097202 (2003).

[5] J. Bekaert, D. Buntinx, C. Van Haesendonck, V. V. Moshchalkov, J. De Boeck, G. Borghs, and V. Metlushko, Appl. Phys. Lett. **81**, 3413 (2002).
[6] S. P. Li, D. Peyrade, M. Natali, A. Lebib, Y. Chen, U. Ebels, L. D. Buda, and K. Ounadjela, Phys. Rev. Lett. **86**, 1102 (2001).
[7] I. A. Campbell and A. Fert, in *Ferromagnetic materials*, edited by E. P. Wohlfarth (North-Holland, Amsterdam, 1982), Vol. 3; T. R. McGuire and R. I. Potter, IEEE Trans. Magn. **11**, 1018 (1975).
[8] OOMMF framework is available at http://gams.nist.gov/oommf
[9] R. D. McMichael and M. J. Donahue, IEEE Trans. Magn. **33**, 4167 (1997).
[10] T. Taniyama, I. Nakatani, T. Namikawa, Y. Yamazaki, Phys. Rev. Lett. **82**, 2780 (1999).
[11] P. M. Levy and S. Zhang, Phys. Rev. Lett. **79**, 5110 (1997).